

Superhydrophobic to Superhydrophilic Wetting Control in Graphene Films

By Javad Rafiee, Mohammad A. Rafiee, Zhong-Zhen Yu, and Nikhil Koratkar*

Superhydrophobic materials with water contact angles above 150° are the key enabler for antisticking, anticontamination, and self-cleaning technologies.^[1–6] Similarly, superhydrophilic materials with water contact angles below 10° have many important applications; for example, as a wicking material in heat pipes and for enhanced boiling heat transfer.^[7,8] In general, the wettability of a solid surface is strongly influenced both by its chemical composition and by its geometric structure (or surface roughness). Several experimental and modeling studies^[9–14] have focused on exploiting surface roughness to engineer superhydrophobicity or superhydrophilicity. Both microscale roughness features (e.g., micromachined silicon pillars) as well as nanoscale features (e.g., aligned arrays of carbon nanotubes) have been investigated. However, so far the wetting properties of graphene-based coatings have not been studied in detail. Graphene is a single-atom-thick sheet of sp^2 hybridized carbon atoms.^[15–18] When deposited on a planer substrate, the individual graphene sheets form an interconnected film, which increases the surface roughness of the substrate by one to two orders of magnitude. We demonstrate here that this roughness effect in conjunction with the surface chemistry of the graphene sheets can be used to dramatically alter the wettability of the substrate. If hydrophilic graphene sheets are used (for example, by sonicating the as-produced graphene in water), the substrate acquires a superhydrophilic character. Conversely if hydrophobic graphene sheets are used (by sonicating the as-produced graphene in acetone) then the roughness effect imparts superhydrophobicity to the underlying substrate. By controlling the relative proportion of acetone and water in the solvent, the contact angle of the resulting graphene film can be tailored over a wide range (from superhydrophobic to superhydrophilic). Such graphene-based coatings with controllable wetting properties provide a facile and effective means to modify the wettability of a variety of surfaces.

The graphene sheets used in this study were extracted from graphite using the method developed in Reference [19,20]. In this method, partially oxygenated graphene sheets are generated by the rapid thermal expansion ($>2000^\circ\text{C min}^{-1}$) of completely

oxidized graphite oxide. The protocols used to oxidize graphite to graphite oxide and then generate graphene sheets (Fig. 1a) by the thermal exfoliation of graphite oxide are provided in the Experimental section. Figure 1b illustrates a transmission electron microscopy (TEM) image of a typical graphene flake synthesized by the above method and deposited on a standard TEM grid for imaging. The flake is several micrometers in dimension; note the wrinkled (rough) surface texture of the graphene flake. Figure 1c displays a high-resolution TEM (HRTEM) image of the edge of a typical graphene flake, indicating that each flake is comprised of ~ 3 individual graphene sheets. The electron diffraction pattern (shown in inset) confirms the signature of few-layered graphene.

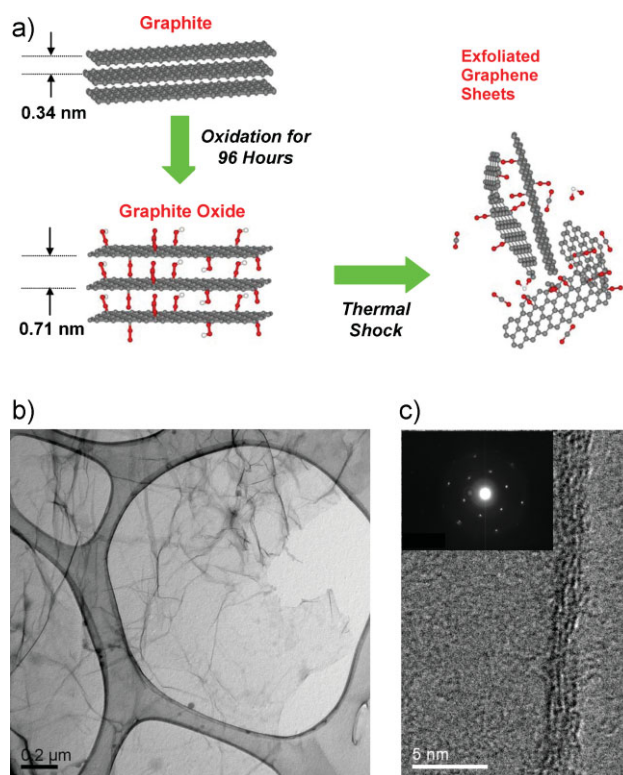


Figure 1. a) Schematic image of the oxidation and thermal exfoliation process used to derive graphene sheets from graphite. b) TEM image of a typical graphene flake. The individual sheets are several micrometers in dimension and show a highly wrinkled (rough) surface topology. c) High-resolution TEM of the sheet edges indicating that each graphene flake is comprised of ~ 3 individual graphene sheets. The electron diffraction pattern shown in the inset confirms the signature of few-layered graphene.

[*] Prof. N. Koratkar, J. Rafiee, M. A. Rafiee
Department of Mechanical, Aerospace, and Nuclear Engineering
Rensselaer Polytechnic Institute, Troy, NY 12180 (USA)
E-mail: koratn@rpi.edu

Prof. Z.-Z. Yu
State Key Laboratory of Chemical Resource Engineering
College of Materials Science and Engineering
Beijing University of Chemical Technology, Beijing 100029 (China)

DOI: 10.1002/adma.200903696

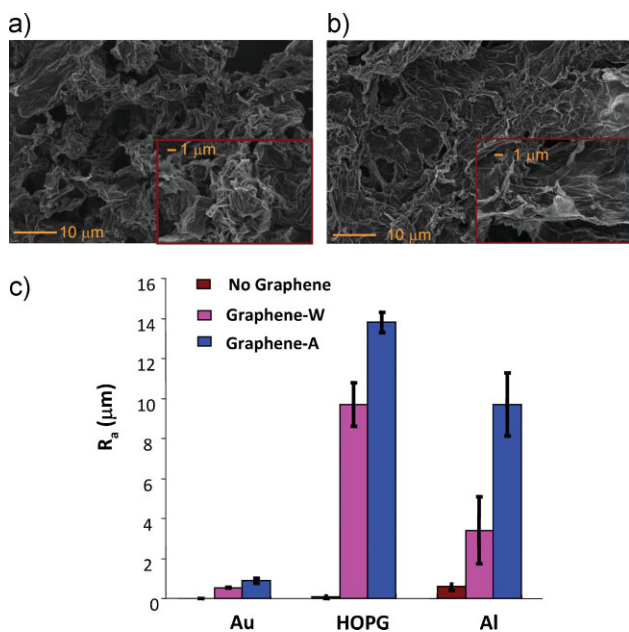


Figure 2. a) SEM image of a graphene film deposited on an Al substrate. Here, acetone is used as the solvent for graphene ultrasonication (graphene-A Film). b) Corresponding SEM image for graphene film deposited on Al substrate but with water as the solvent used to ultrasonicate graphene (graphene-W Film). c) The average surface-roughness parameter (R_a) for Al, Au, and HOPG substrates is compared before and after graphene-W and graphene-A film deposition. The graphene film enhances the surface roughness of the underlying substrate by one to two orders of magnitude.

In order to disperse the graphene sheets on a substrate, we perform high-power ultrasonication of the graphene sheets in a suitable solvent^[21] such as water or acetone. The desired amount of graphene sheets was first weighed and dispersed in the solvent (ratio of 100 mL solvent to 0.05 g graphene) using an ultrasonic probe sonicator at high amplitude (Sonics Vibracell VC 750, Sonics and Materials Inc., USA) for 1 h. To deposit the graphene film, $\sim 10\text{ cm}^3$ of the suspension was gently released on the substrate by a dropper in a clean-room environment and allowed to dry for 12 h in a fume hood for evaporation of the solvent. Subsequently, the surfaces were further cleaned using nitrogen gas. Scanning electron microscopy (SEM) images of graphene films deposited on an aluminum (Al) substrate by this technique are shown in Figure 2a, for water as the solvent, and in Figure 2b, with acetone as the solvent. To determine the average roughness of the graphene films, we used a Dektak Surface Profilometer (from VEECO); at least five separate measurements were performed for each sample for statistics. Figure 2c shows the measured surface-roughness parameter (R_a) for aluminum (Al), gold (Au), and highly ordered pyrolytic graphite (HOPG) substrates before and after deposition of graphene films with pure water as the solvent (graphene-W film) and with pure acetone as the solvent (graphene-A film). The error bars in Figure 2c represent the standard deviation with respect to the mean value. The graphene-coated samples show one to two orders of magnitude increase in the average surface roughness as compared to the baseline substrates prior to graphene deposition. The average surface roughness of graphene-A films was also

observed to be larger than those of graphene-W films. This is also confirmed by the high-resolution SEM images (insets in Fig. 2a and 2b); the sheets in the graphene-W film appear to spread out more and partially align with the underlying substrate and are therefore smoother in comparison to the graphene-A film.

We performed static contact angle measurements by placing a droplet of deionized water on the surface of the various substrates. The contact angle was measured using a Ramé-Hart M500 digital goniometer equipped with a dispensing needle (VICI Precision Sampling Co., CA, USA). A $1\ \mu\text{L}$ water droplet was generated using the automatic dispenser of the goniometer, based on four time-controlled volume steps of $0.25\ \mu\text{L}$ close to the sample surface. The sessile droplet was formed by fixing the needle and approaching the substrate parallel to the needle direction with a very gentle feed rate of a few micrometers per minute. All the tests were performed in the air at room temperature ($\sim 74^\circ\text{F}$). The axisymmetric-drop-shape analysis profile (ADSA-P) method was used for estimating the contact angle of water on the solid surface.

For the Au substrate (Fig. 3a), we find that the contact angle of the baseline Au (without graphene film coating) is $\sim 76.3^\circ$. When graphene sonicated in water (graphene-W) was deposited on the substrate, we observed complete wetting, i.e., the water droplet brought into contact with the solid spontaneously formed a film with a water contact angle of $\sim 0^\circ$. The graphene-W film therefore displays extreme superhydrophilicity. The opposite effect was observed with graphene sheets sonicated in acetone (graphene-A); the water contact angle of the Au substrate with graphene-A coating was observed to lie in the superhydrophobic range ($\sim 160^\circ$). Identical behavior was reproduced for HOPG (Fig. 3b) and also for Al (Fig. 3c) substrates. Films comprised of graphene-W imparted superhydrophilicity to the Al and HOPG substrate, while graphene-A-based coatings imparted superhydrophobicity to the underlying substrate. By combining water and acetone in various proportions (e.g., 1:1 to 1:10) as the solvent, we were also able to tailor the water contact angle of the resulting graphene films over a wide range, as illustrated in Figure 3d.

To explain these results, we consider the Wenzel model^[22] for water droplets placed on rough surfaces. In the Wenzel model, the apparent contact angle on a rough surface in the homogeneous regime, θ_w is expressed as:

$$\cos \theta_w = r(\cos \theta) \quad (1)$$

where θ is the contact angle on the flat surface and r is the roughness ratio, defined as the ratio of the true area of the solid surface to its projection area. Since the r is always larger than 1, from Equation (1) it is clear that, θ_w will be higher than θ if the surface is originally hydrophobic ($\theta > 90^\circ$), otherwise, θ_w is lower than θ . In other words, the roughness effect amplifies the inherent wettability of the substrate material. Therefore if an individual graphene-W sheet is hydrophilic, then a rough graphene-W film (Fig. 2c) is expected to be superhydrophilic and, conversely, if an individual graphene-A sheet is hydrophobic, then the Wenzel model predicts that a rough film (Fig. 2c) comprised of graphene-A sheets would display superhydrophobic response.

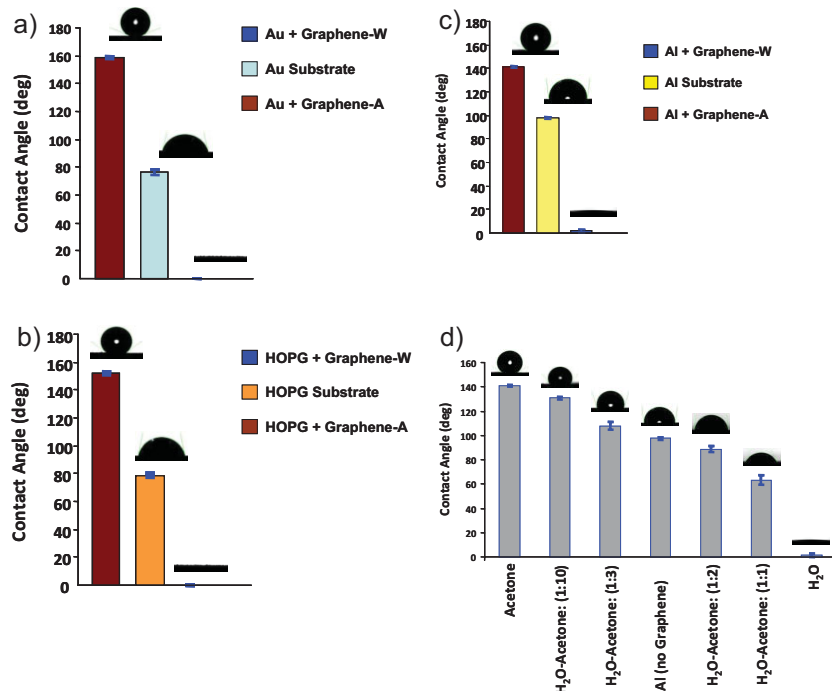


Figure 3. a) The water contact angle of the baseline Au substrate is $\sim 76.3^\circ$, which is increased to $\sim 160^\circ$ by graphene-A deposition and decreased to $\sim 0^\circ$ by graphene-W deposition. b) For the HOPG substrate the baseline contact angle is $\sim 81.5^\circ$, which is increased to $\sim 151.4^\circ$ by graphene-A deposition and decreased to $\sim 0^\circ$ by graphene-W deposition. c) Corresponding results for an Al substrate showing a variation in contact angle from $\sim 97.5^\circ$ for baseline Al to $\sim 142.1^\circ$ for the graphene-A film and $\sim 1.6^\circ$ for the graphene-W film. d) Tailoring of the contact angle of an Al substrate by ultrasonating graphene sheets in a water/acetone mixture. Increasing the relative proportion of water in the mixture results in more hydrophilic behavior, while, conversely, higher acetone content yields more hydrophobic response.

The as-produced graphene-W is expected to have carbonyl and carboxyl groups attached to the sheet edges^[19,20,23] which will make graphene-W hydrophilic due to the presence of carbon-oxygen bonds.^[24] To understand why graphene-A are hydrophobic we performed reflectance-mode Fourier transform infrared (FTIR) spectroscopy measurements on the various graphene samples produced in this study. The measurements were carried out in a Varian spectrometer with a variable-angle specular reflectance accessory. The results reported here were obtained from 128 scans at a 4 cm^{-1} resolution and were verified at least four times with different samples prepared and stored under identical conditions. The results (Fig. 4a) indicate chemisorption of acetone on graphene for graphene-A films as evidenced by symmetric and asymmetric CH_3 stretching peaks^[25] at ~ 2875 and $\sim 2964\text{ cm}^{-1}$, respectively. Similarly we observe symmetric and asymmetric CH_2 stretching peaks (Fig. 4a) at ~ 2852 and $\sim 2931\text{ cm}^{-1}$, respectively, for the graphene-A film. No such peaks are detected in the FTIR spectra of graphene-W samples as indicated in Figure 4b.

Chemisorption of acetone on defective carbon nanotubes has been previously reported,^[25] acetone is adsorbed on the nanotube walls via C–O–C type bonds, in configurations where the terminal methyl (CH_3) groups point away from the nanotube surfaces. This view is also supported by ab initio calculations based on density functional theory showing that acetone attaches

preferentially at defects, such as vacancies on nanotube sidewalls, via $\sim 0.90\text{--}3.3\text{ eV}$ interactions resulting from C(acetone)–O–C (nanotube) bonds, rather than C=O bonds, on nanotube surfaces.^[26] For graphene sheets, defects (i.e., dangling bonds) are ubiquitous along the sheet edges. Moreover the thermal shock that was employed to exfoliate graphite oxide to graphene leaves the structure littered with defects, such as five- and seven-membered rings and carbon vacancies.^[27] Furthermore, ultrasonication may also create new defects on the graphene basal planes, thereby facilitating the chemisorption of acetone. It is well established^[28] that the carbon–hydrogen bond is hydrophobic in nature and hence the attachment of terminal methyl groups to graphene will impart a net hydrophobic character to graphene-A. Our group has previously reported^[24] a superhydrophobic to hydrophilic transition in aligned multi-walled carbon nanotube arrays by electrochemical oxidation of the nanotube surface; however, to the best of our knowledge, the effect of acetone chemisorption of the wettability of carbon nanotubes has not been studied. In general, one would expect the hydrophobicity of carbon nanotubes to be enhanced by the chemisorption of acetone, however this effect is likely to be far more powerful in graphene due to its enhanced active surface area. In nanotubes mainly the outer surface of the tube is exposed to acetone/water molecules, while in graphene sheets

both the top and bottom surfaces of the sheet are exposed to the surrounding medium. Moreover graphene that is thermally reduced from graphite oxide has a high density of defects^[27] along its basal planes, which greatly enhances its chemical reactivity and facilitates the chemisorption of acetone.

To summarize, we have demonstrated a facile technique to control the wettability of a solid surface by the deposition of a graphene film on the surface. Depending on whether water, acetone, or a combination of water and acetone is used as the solvent, the contact angle of the surface can be tailored over a wide range from superhydrophobic to superhydrophilic behavior.

Experimental

Natural graphite flakes with an average diameter of $48\ \mu\text{m}$ were supplied from Huadong Graphite Factory (Pingdu, China). Concentrated sulfuric acid (95–98%), concentrated nitric acid (68%), and hydrochloric acid (36–38%) were purchased from Beijing Chemical Factory (China). Potassium chlorate (99.5%) was obtained from Fuchen Chemical Reagents (Tianjin, China).

Graphite oxide was prepared by oxidizing graphite in a solution of sulfuric acid, nitric acid, and potassium chlorate for 96 h based on the work of Aksay and co-workers [19,20]. X-Ray diffraction patterns of natural graphite and graphite oxide are provided in the Supporting Information. Thermal exfoliation of graphite oxide was achieved by placing the graphite

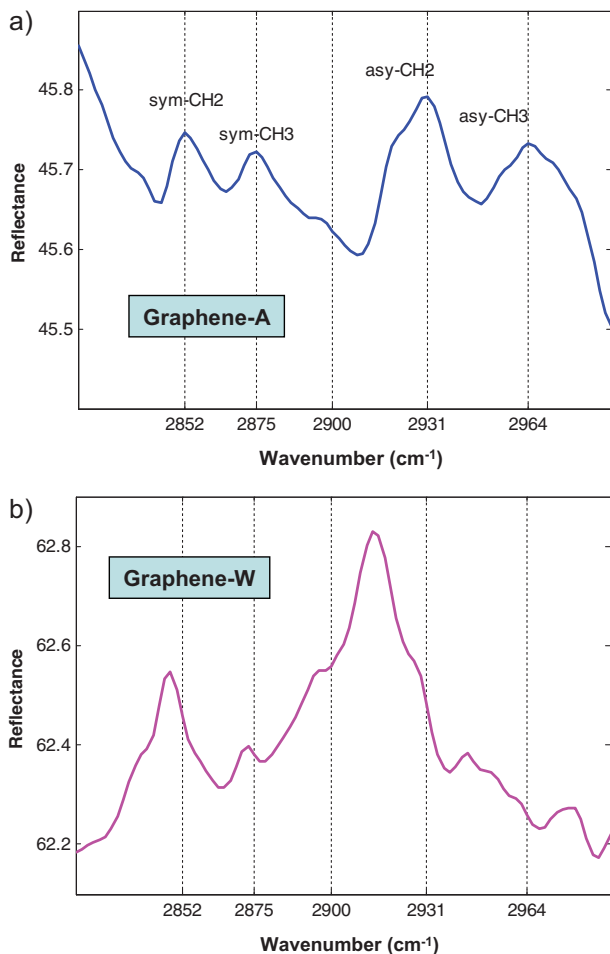


Figure 4. a) Typical FTIR spectrum of a graphene-A-type sample indicating peaks at ~ 2875 and ~ 2964 cm^{-1} corresponding to CH_3 symmetric and asymmetric stretching modes, respectively. Similarly, peaks are also observed at ~ 2852 and ~ 2931 cm^{-1} corresponding to the CH_2 symmetric and asymmetric stretching modes, respectively. b) FTIR spectrum of a typical graphene-W sample. No peaks in the spectra corresponding to CH_3 and CH_2 modes are detected for this case.

oxide powder (200 mg) in a 200-mm-inner-diameter, 1-m-long quartz tube that was sealed at one end. The other end of the quartz tube was closed using a rubber stopper. An argon inlet was then inserted through the rubber stopper. The sample was flushed with argon for 10 min, and the quartz tube was quickly inserted into a tube furnace (Thermolyne 79300, Thermo Fisher Scientific Inc., USA) preheated to 1050°C and held in the furnace for 30 s. Rapid heating ($>2000^\circ\text{C min}^{-1}$) splits the graphite oxide into bulk quantities of few-layered graphene sheets.

Acknowledgements

N.K. acknowledges funding support from the US Office of Naval Research (Award Number: N000140910928) and the US National Science

Foundation (Award Number: 0900188). Supporting Information is available online from Wiley InterScience or from the author.

Received: October 28, 2009

Revised: November 19, 2009

Published online: March 8, 2010

- [1] A. Lafuma, D. Quere, *Nat. Mater.* **2003**, *2*, 457.
- [2] R. Furstner, W. Barthlott, *Langmuir* **2005**, *21*, 956.
- [3] R. Blossey, *Nat. Mater.* **2003**, *2*, 301.
- [4] R. Furstner, W. Barthlott, C. Neinhuis, M. Miwa, A. Nakajima, A. Fujishima, K. Hashimoto, T. Watanabe, *Langmuir* **2000**, *16*, 5754.
- [5] Y. Cheng, D. E. Rodak, *Appl. Phys. Lett.* **2005**, *86*, 144101.
- [6] X. J. Feng, L. Jiang, *Adv. Mater.* **2006**, *18*, 3063.
- [7] L. Chen, Z. Wang, P. I. Wang, Y. Peles, N. Koratkar, G. P. Peterson, *Small* **2008**, *5*, 1403.
- [8] R. Chen, M. Lu, V. Srinivasan, Z. Wang, H. H. Cho, A. Majumdar, *Nano Lett.* **2009**, *9*, 548.
- [9] A. Otten, S. Herminghaus, *Langmuir* **2004**, *20*, 2405.
- [10] N. A. Patankar, *Langmuir* **2003**, *19*, 1249.
- [11] Z. Wang, C. Lopez, A. Hirs, N. Koratkar, *Appl. Phys. Lett.* **2007**, *91*, 023105.
- [12] Z. Wang, Y. Ou, T.-M. Lu, N. Koratkar, *J. Phys. Chem. B* **2007**, *111*, 4296.
- [13] Z. Wang, L. Ci, P. Ajayan, N. Koratkar, *Appl. Phys. Lett.* **2007**, *90*, 143117.
- [14] L. Zhu, Y. Xiu, J. Xu, P. A. Tamirisa, D. W. Hess, C. P. Wong, *Langmuir* **2005**, *21*, 11208.
- [15] J. C. Meyer, A. K. Geim, M. I. Katsnelson, K. S. Novoselov, T. J. Booth, S. Roth, *Nature* **2007**, *446*, 60.
- [16] J. S. Bunch, A. M. Van Der Zande, S. S. Verbridge, I. W. Frank, D. M. Tanenbaum, J. M. Parpia, H. G. Craighead, P. L. McEuen, *Science* **2007**, *315*, 490.
- [17] C. N. R. Rao, A. K. Sood, K. S. Subrahmanyam, A. Govindaraj, *Angew. Chem. Int. Ed.* **2009**, *48*, 7752.
- [18] C. Lee, X. Wei, J. W. Kysar, J. Hone, *Science* **2008**, *321*, 385.
- [19] H. C. Schniepp, J.-L. Li, M. J. McAllister, H. Sai, M. Herrera-Alonso, D. H. Adamson, R. K. Prud'homme, R. Car, D. A. Saville, I. A. Aksay, *J. Phys. Chem. B* **2006**, *110*, 8535.
- [20] M. J. McAllister, J.-L. Li, D. H. Adamson, H. C. Schniepp, A. A. Abdala, J. Liu, M. Herrera-Alonso, D. L. Milius, R. Car, R. K. Prud'homme, I. A. Aksay, *Chem. Mater.* **2007**, *19*, 4396.
- [21] S. Park, J. A. An, I. Jung, R. D. Piner, S. J. An, X. Li, A. Velamakanni, R. S. Ruoff, *Nano Lett.* **2009**, *9*, 1593.
- [22] R. N. Wenzel, *Ind. Eng. Chem.* **1936**, *28*, 988.
- [23] S. Stankovich, D. A. Dikin, D. Dommett, K. Kohlhaas, E. J. Zimney, E. A. Stach, R. D. Piner, S. T. Nguyen, R. S. Ruoff, *Nature* **2006**, *442*, 282.
- [24] Z. Wang, L. Ci, L. Chen, S. Nayak, P. M. Ajayan, N. Koratkar, *Nano Lett.* **2007**, *7*, 697.
- [25] A. V. Ellis, K. Vijayamohan, R. Goswami, N. Chakrapani, L. S. Ramanathan, P. M. Ajayan, G. Ramanath, *Nano Lett.* **2003**, *3*, 279.
- [26] N. Chakrapani, Y. M. Zhang, S. K. Nayak, J. A. Moore, D. L. Carroll, Y. Y. Choi, P. M. Ajayan, *J. Phys. Chem. B* **2003**, *107*, 9308.
- [27] K. N. Kudin, B. Ozbas, H. C. Schniepp, R. K. Prud'homme, I. A. Aksay, R. Car, *Nano Lett.* **2007**, *8*, 36.
- [28] J. Kyte, *J. Biophys. Chem.* **2003**, *100*, 193.